

Effective hard x-ray spectrum of a tabletop Mather-type plasma focus optimized for flash radiography of metallic objects

V. Raspa, C. Moreno, L. Sigaut, and A. Clausse

Citation: [Journal of Applied Physics](#) **102**, 123303 (2007); doi: 10.1063/1.2822449

View online: <http://dx.doi.org/10.1063/1.2822449>

View Table of Contents: <http://scitation.aip.org/content/aip/journal/jap/102/12?ver=pdfcov>

Published by the [AIP Publishing](#)

Articles you may be interested in

[Anomalous resistivity effect on multiple ion beam emission and hard x-ray generation in a Mather type plasma focus device](#)

[Phys. Plasmas](#) **18**, 103302 (2011); 10.1063/1.3647958

[Current sheath behavior and its velocity enhancement in a low energy Mather-type plasma focus device](#)

[J. Appl. Phys.](#) **109**, 043301 (2011); 10.1063/1.3549017

[Tailoring a plasma focus as hard x-ray source for imaging](#)

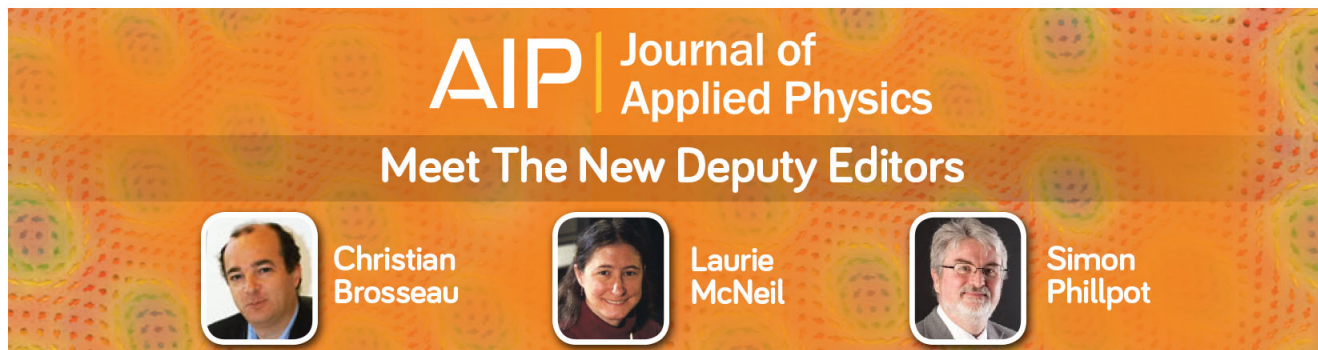
[Appl. Phys. Lett.](#) **96**, 031501 (2010); 10.1063/1.3291039

[Hard x-ray source for flash radiography based on a 2.5 kJ plasma focus](#)

[J. Appl. Phys.](#) **102**, 033304 (2007); 10.1063/1.2767829




[Plasma-focus-based tabletop hard x-ray source for 50 ns resolution introspective imaging of metallic objects through metallic walls](#)

[Appl. Phys. Lett.](#) **89**, 091502 (2006); 10.1063/1.2335631



AIP | Journal of Applied Physics

Meet The New Deputy Editors

	Christian Brosseau		Laurie McNeil		Simon Phillpot
---	---------------------------	---	----------------------	---	-----------------------

Effective hard x-ray spectrum of a tabletop Mather-type plasma focus optimized for flash radiography of metallic objects

V. Raspa^{a)} and C. Moreno

Departamento de Física, FCEyN-UBA, PLADEMA-CNEA, and INFIP-CONICET, Pab. 1, Ciudad Universitaria, (1428) Buenos Aires, Argentina

L. Sigaut

Departamento de Física, FCEyN-UBA, Pab. 1, Ciudad Universitaria, (1428) Buenos Aires, Argentina

A. Clausse

Universidad Nacional del Centro, PLADEMA-CNEA and CONICET, Campus Universitario, Paraje Arroyo Seco, (7000) Tandil, Buenos Aires, Argentina

(Received 8 June 2007; accepted 20 October 2007; published online 19 December 2007)

The effective spectrum of the hard x-ray output of a Mather-type tabletop plasma focus device was determined from attenuation data on metallic samples using commercial radiographic film coupled to a $\text{Gd}_2\text{O}_2\text{S}:\text{Tb}$ phosphor intensifier screen. It was found that the radiation has relevant spectral components in the 40–150 keV range, with a single maximum around 60–80 keV. The radiation output allows for 50 ns resolution, good contrast, and introspective imaging of metallic objects even through metallic walls. A numerical estimation of the induced voltage on the focus during the compressional stage is briefly discussed. © 2007 American Institute of Physics.

[DOI: 10.1063/1.2822449]

I. INTRODUCTION

The use of plasma focus x rays for radiographic imaging, known at least since 1976,¹ is now an attractive area of applied research on which many interesting results were produced. Radiographs of either biological specimens^{2,3} or small samples^{4–7} were recently obtained using low-energy Mather-type plasma focus devices as radiation sources. Important contributions to the field were also made tailoring tabletop x pinches to get, for instance, a high-definition radiograph of a house fly⁸ or a phase-contrast radiography of inertial confinement fusion capsules.^{9,10} In all of the above-mentioned studies, mainly the soft region of the x-ray spectrum was taken advantage of.

The use of the hard x-ray emission ($h\nu \sim 100$ keV) from a plasma focus for producing nonconventional introspective imaging of metallic objects was reported in 2000.¹¹ Figures 1 and 2, respectively, show digitized images of a metallic BNC tee connector, and a 10-mm-thick aluminum block with two 1/4–20 bolts, made of steel (left) and brass (right), screwed on it. Both radiographies were taken with a single plasma focus shot, through a 9-mm-thick iron flange. The dark circle near the upper left of each image is a through hole made on the flange, close to its border. These results are neat examples of the possibilities that plasma focus devices can offer to hard x-ray imaging. Additional examples can be seen in Ref. 12. More recently, a tabletop plasma focus facility was used as a hard x-ray source for 50 ns resolution radiography of metallic objects either in fast rotation¹³ or through as much as 22-mm-thick metallic walls.¹⁴

While the spectral characteristics of the soft x-ray output of plasma focus devices were intensively investigated in

great detail, the spectrum of the radiation involved in the above-mentioned hard x-ray applications received less attention. In our device, for instance, the involved radiation was characterized only by a measured effective average energy of about 100 keV.¹⁴ In other facilities, studies were conducted to determine the spectra above 5 keV using Ross filters^{15–17} as well as Ilford nuclear emulsions.^{16,18} Ross filters enabled the exploration of the 5.0–67.4 keV energy range¹⁷ (the uppermost energy limit being the tantalum *K*-shell absorption edge), but not beyond that. Such an energy window was adequate for the studied devices, but it is clearly unsuitable for the 100 keV region. To determine the photon spectrum using nuclear emulsions is, in turn, quite an indirect process whose results are useful to describe the general trend of the high-energy tail of the spectrum (above ~ 150 keV), but they are inadequate to describe the low-energy region.¹⁸ More recently, Tartari¹⁹ *et al.* measured the hard x-ray output

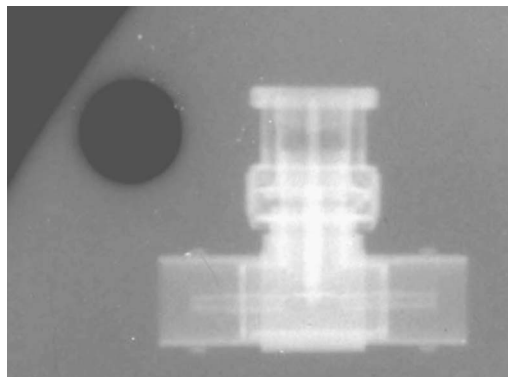


FIG. 1. Digitized radiograph of a metallic BNC tee connector imaged with a single plasma focus shot, through a 9-mm-thick iron flange. The dark circular region near the upper left of the connector is a through hole made on the flange, close to its border.

^{a)}Electronic mail: raspa@df.uba.ar.

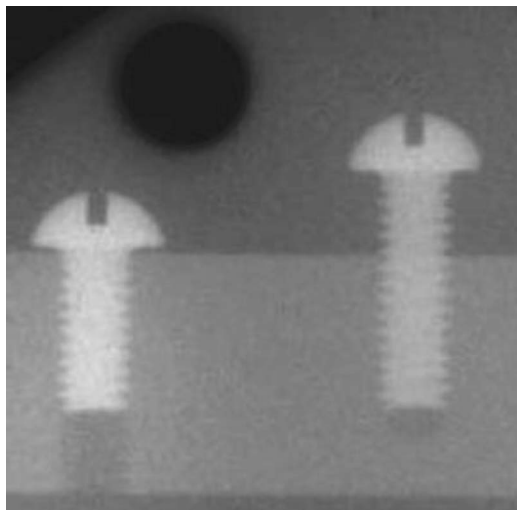


FIG. 2. A 10-mm-thick aluminum block with two 1/4–20 bolts, one made of steel (left) and the other of brass (right), imaged with a single plasma focus shot through a 9-mm-thick iron flange. The dark circular region near the upper left of the block is a through hole made on the flange, close to its border.

spectrum of a 7 kJ 0.5 MA plasma focus using a multichannel differential absorption spectrometer based on thermoluminescence dosimeters (TLDs). The spectrometer was exposed to about 40 shots in order to obtain a good signal-to-noise ratio. The resulting spectra exhibit a prominent peak near 10 keV, with a 5 keV full width at half-maximum (FWHM), followed by a tail of much lower intensity extended from 15 to 45 keV.

Efforts were also made to characterize the angular distribution of the plasma focus hard x-ray emission. Castillo *et al.*,² for instance, measured the hard x-ray dose for energies above 25 keV in a 2 kJ 31 kV plasma focus, using TLDs. They measured that at a distance of 1 m from the focus, the hard x-ray dose on axis is about 0.1 mrad per shot and it does not vary for half aperture angles smaller than 5 degrees from the electrodes axis. More recently and also using TLDs, Castillo *et al.*²⁰ found that the x-ray emission of a 4.8 kJ 37 kV plasma focus shows a bimodal angular distribution peaked at ± 20 degrees from the electrodes axis, for emitted photons of above 15 keV.

The knowledge of the hard x-ray output spectrum is important for the development of applications and also for cross-checking complex issues associated with physical processes occurring in the focus. Validation of numerical codes could also benefit from it. For these reasons, the effective hard x-ray spectrum of our device was measured on a single shot basis, and it is reported below.

II. DEVICE

A small-chamber Mather-type plasma focus device was studied as a pulsed hard x-ray source. The facility is powered by a capacitor bank formed by 18 Maxwell capacitors model 31161 (0.7 μF each) connected in parallel and charged up to 30 kV (5.7 kJ of stored energy). Under these conditions, it drives a peak current of 360 kA in a quarter-period of 1.25 μs to the discharge chamber. The capacitor bank foot-

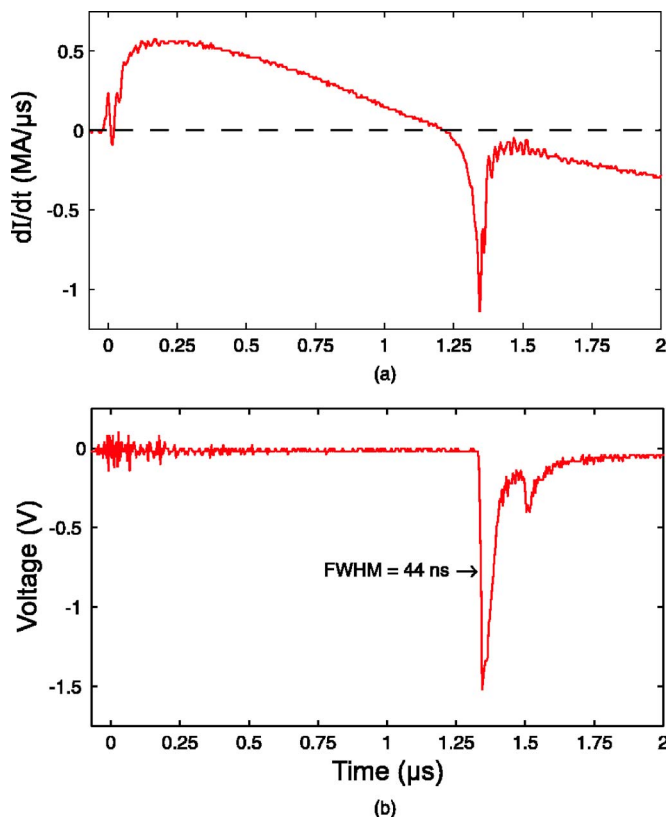


FIG. 3. (Color online) (a) Nonintegrating Rogowski coil signal showing the time derivative of the discharge current. (b) Photomultiplier signal showing hard x-ray and neutron production.

print and height are 0.60 m^2 and 1 m, respectively. Deuterium at 4 mbar was used as working gas since it maximizes the hard x-ray production and the shot-to-shot regularity for this device. The coaxial electrodes are formed by a hollow copper anode (central electrode) surrounded by a squirrel-cage-like bronze cathode. They are separated by a Pyrex insulator and located coaxially inside a 1 dm^3 stainless steel cylindrical chamber with a 2-mm-thick wall. The anode is a tube of 38 mm outer diameter with a 2-mm-thick wall, and is 85 mm in length, whereas the cathode is formed by eight brass rods, each one 3 mm in diameter and 87 mm in length, located equally spaced around a circle 37 mm in diameter concentric with the anode. The insulator sleeve is 50 mm in outer diameter with 4-mm-thick walls, and is 34 mm in length. The output window for the hard x-ray radiation is a 1.25-mm-thick stainless steel flat disk, which is also the front end of the cylindrical chamber. A nonintegrating Rogowski coil and a photomultiplier tube coupled to a 5-cm-thick and 5-cm-diam NE102A plastic scintillator were used to monitor the discharge. Figure 3(a) illustrates a Rogowski coil signal showing the focalization dip at 1.34 μs . The photomultiplier signal is exposed in Fig. 3(b), from which a 44 ns FWHM can be inferred for the x-ray peak registered in time correspondence with the focalization dip. A second photomultiplier peak, corresponding to the neutron emission, is detected with a time-of-flight delay of 100 ns.

III. METHOD

The pulsed hard x-ray radiation is emitted as a consequence of the collision against the anode base of highly en-

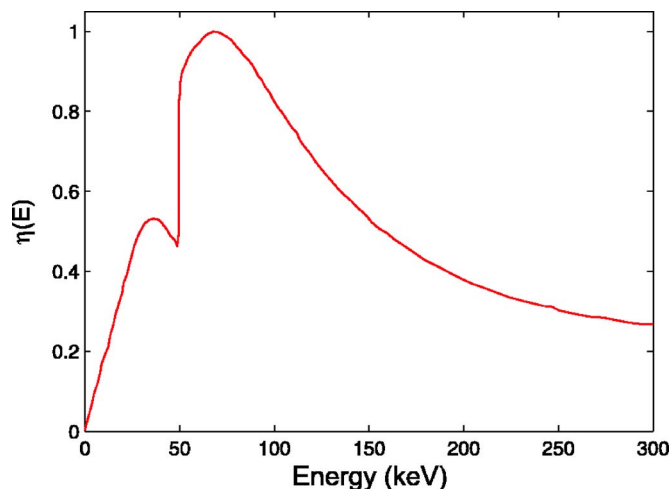


FIG. 4. (Color online) Normalized conversion efficiency of the intensifier screen as a function of the incident photon energy.

ergetic electron beams accelerated as a result of the plasma focalization. The extremely short wavelength of the involved radiation (~ 10 pm, or $h\nu \sim 100$ keV) together with the very short pulse width (~ 50 ns FWHM) make both crystal spectrometers and single-event gamma spectroscopy unsuitable for its spectral analysis. Therefore, the differential absorption method was followed to determine its spectrum.

High sensitivity orthochromatic Agfa x-ray film along with a terbium-doped gadolinium oxysulfide ($\text{Gd}_2\text{O}_2\text{S:Tb}$) intensifying screen, which is one of the most widely used film-screen sets for general purpose radiography as well as for hard x-ray imaging,^{11–14} was used as a hard x-ray detector.

In these detectors, the x-ray film is impressed by visible photons emitted by the intensifying screen, which acts basically as a transducer from hard x rays to visible light. This conversion process is due to interactions in the $\text{Gd}_2\text{O}_2\text{S:Tb}$ phosphor. The x-ray film itself is placed inside a visible light tight plastic cassette whose internal walls are coated by individual soft thin pads that contain the $\text{Gd}_2\text{O}_2\text{S:Tb}$ transducer. Such pads are commonly referred to as intensifier screens.

The normalized conversion efficiency of the intensifier screen as a function of the incident photon energy, $\eta(E)$, is shown in Fig. 4. Absolute values of the screen conversion efficiency can be found in Ref. 21. The visible light emitted by the intensifier screen has a band spectrum dominated by photons of ~ 540 nm (green), with the next two relevant bands being located at 480 and 580 nm, respectively, each one with a relative intensity of 0.34 with respect to the maximum.²²

The spectral sensitivity of the orthochromatic x-ray film spans from 300 to 580 nm, and therefore matches the spectral output of the intensifier screen. The film itself is insensitive to hard x rays and to wavelengths longer than 650 nm (red).

The hard x-ray effective spectrum $S(E)$ can be inferred from the attenuation the beam experiences when passing through samples of different materials and thicknesses. For any arbitrary sample thickness d , the transmission coefficient $T(d)$ is defined by

$$T(d) \equiv \frac{I(d)}{I_0} = \frac{\int_0^\infty \eta(E)S(E)e^{-k(E)d}dE}{\int_0^\infty \eta(E)S(E)dE}, \quad (1)$$

where $I_0=I(0)$ and $I(d)$ represent the incident and transmitted intensities, respectively. Expression (1) holds under the hypothesis that the intensity of each spectral component decays exponentially as it penetrates matter. In that case, a linear attenuation coefficient, $k(E)$, depending also on the sample material, characterizes the radiation decay. Values of $k(E)$ from 1 keV to 20 MeV for elements $Z=1$ to 92 are tabulated in Ref. 23.

Experimental values, T_{ij}^{exp} , of the $I(d)/I_0$ ratio were determined by radiographing, with a single shot, a set of plates made with the materials and thicknesses detailed in Table I. Subindexes i and j label materials and thicknesses, respectively. Each T_{ij}^{exp} value was obtained from the corresponding measured film optical density (OD) and the film exposure response.²⁴ A function $S(E)$ was inferred afterwards from Eq. (1), using the zeroth-order regularization method.²⁵

IV. RESULTS

Figure 5 shows a radiograph of the above-mentioned set of plates. It was taken in a single plasma focus shot, placing the object outside the chamber, at 40 cm from the chamber front wall. Different tonalities can be appreciated according to the plate material and thickness.

Figure 6 illustrates the measured film optical density for the copper samples as a function of the sample thickness d . Aside from corroborating that thicker samples produce lighter tonalities, and correspondingly lower optical densities, it shows that the film exposure was above the film fog level (which corresponds to $\text{OD}=0.2$) and well below the saturation level ($\text{OD}=3.5$).

The obtained spectrum together with the corresponding error bands are presented in Fig. 7 as full and dashed lines, respectively. As can be observed, the spectral amplitude is

TABLE I. Materials and thicknesses of the used samples. Thickness uncertainties are ± 0.01 cm.

Material	Thicknesses (cm)				
Cadmium			0.11	0.22	0.33
Copper	0.11	0.22	0.33	0.44	0.55
Nickel		0.16	0.27	0.43	0.54
Titanium		0.36	0.44	0.56	0.68
Lead			0.31	0.62	0.93

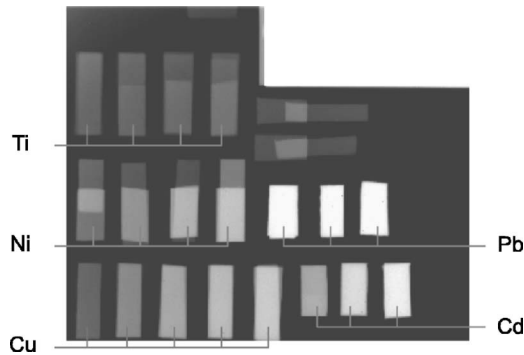


FIG. 5. Single-shot radiographic image of the plates set used to determine the radiation spectrum.

practically null below 40 keV. It then rapidly grows at higher energies, reaching a single maximum located close to 70 keV, and finally it decays until becoming negligible beyond 175 keV. For nickel and titanium, and also for different analyzed images, the obtained spectral profiles are concordant to each other. Cadmium samples were used for cross-checking and the lead ones were used to determine the darkening level of reference corresponding to null exposure. The small bump appearing at 250 keV is a numerical artifact always present at the higher end of the energy range explored during the numerical resolution of Eq. (1).

The error bands were estimated by means of the Monte Carlo method.²⁵ The input data (that is, the measured values of $T_{i,j}^{\text{exp}}$ as well as the corresponding thicknesses j) were randomly perturbed within their own error bands for each material i . Afterwards, a perturbed spectrum $S_n(E)$ was evaluated from such simulated data. A number of $n=1000$ realizations of these calculations gave a set of spectra $S_n(E)$, $1 \leq n \leq 1000$, which, once plotted together with $S(E)$, gave a broad region, delimited by the dashed curves reported as error bands in Fig. 7.

To verify that the measured effective spectrum is compatible with what can be expected for the voltage drop in the focus, $V_p(t)$, such voltage was estimated, neglecting plasma resistivity, as

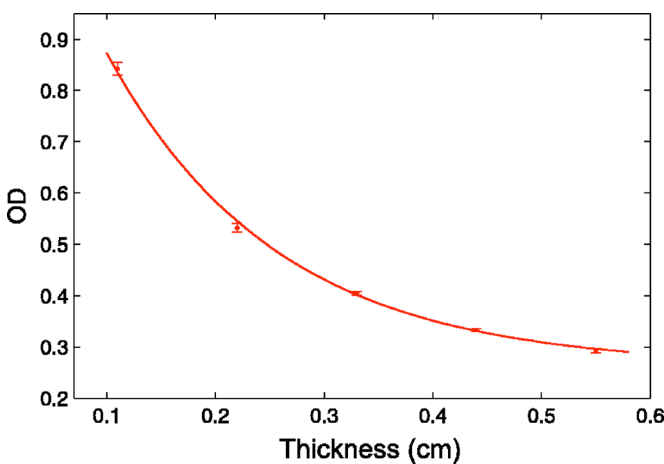


FIG. 6. (Color online) Measured film optical density for the copper samples as a function of the sample thickness.

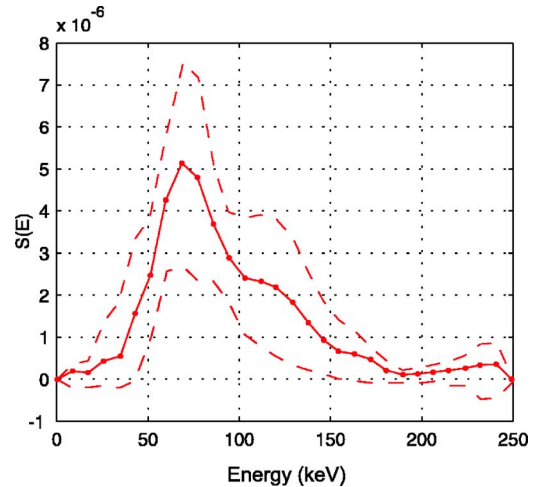


FIG. 7. (Color online) Obtained x-ray spectrum from the copper set of samples. Dashed curves indicate error bands.

$$V_p(t) = \frac{d}{dt}[L_p(t)I(t)], \quad (2)$$

where $I(t)$ is the total current circulating through the pinch and $L_p(t)$ represents the pinch inductance, which in turn was estimated as

$$L_p(t) = \frac{\mu_0 h(t)}{2\pi} \ln \frac{r_e}{r(t)}, \quad (3)$$

where $h(t)$ and $r(t)$ are the pinch length and radius, respectively, and r_e represents the radius of the external electrode. The temporal dependence of $L_p(t)$ and $I(t)$ was evaluated resorting to the well known Lee model.²⁶

Figure 8 shows the calculated temporal evolution of V_p considering a filling pressure of 4 mbar and a charging voltage of 30 kV. According to this model, a voltage peak of approximately 180 kV can be expected during the focus, shortly before the maximum compression occurs. For this reason, a measured spectrum whose relevant components are below 175 kV is considered to be compatible with what can be expected from a validated numerical code.

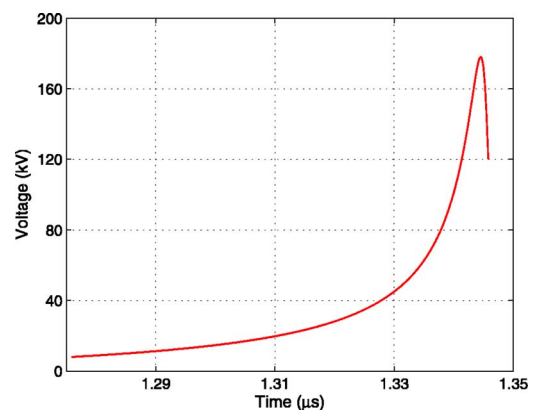


FIG. 8. (Color online) Numerical result for the time evolution of the induced voltage on the pinch during its compression phase, the time being measured from the onset of the discharge current. Filling pressure: 4 mbar of deuterium.

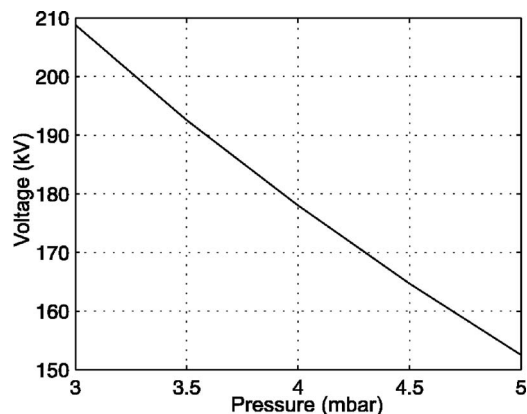


FIG. 9. Calculated dependence of the maximum pinch voltage on the deuterium filling pressure.

Calculations also show that during the plasma radial convergence, V_p is dominated by the $dr(t)/dt$ term involved in Eqs. (2) and (3), such that higher induced voltages in the pinch correspond with higher radial convergence speeds. This fact illustrates the convenience of using lighter filling gases and/or lower pressures in order to increase V_p . In our case, $dr(t)/dt$ reaches an extreme value of $-49 \text{ cm}/\mu\text{s}$ at a filling pressure of 4 mbar.

Figure 9 shows the calculated pressure dependence of the maximum induced voltage, V_{pM} , keeping constant the anode length. It can be seen, as expected, that V_{pM} decreases with the filling pressure in the displayed range. To consider a broader pressure interval while keeping the anode length constant makes little sense, since then the machine starts to be nonoptimized for focalization.

V. FINAL REMARKS AND CONCLUSIONS

The effective hard x-ray spectrum of a Mather-type plasma focus device was measured from attenuation data on metallic samples, within a spectral window for which experimental data were not yet available in the published literature. The resulting spectrum presents a maximum around 60–80 keV and a spectral bandwidth covering the 40–150 keV region. The obtained lower-energy limit is consistent with the fact that spectral components below 40 keV are strongly attenuated by the chamber front wall. Previous experimental results demonstrate that the examined radiation is well suited for good contrast radiography of different materials, as can be appreciated in Figs. 1 and 2. This fact, compatible with a broadband probing radiation, is consistent with the obtained spectrum.

Conventional radiotherapy tubes produce weighted mean photon energies between 66 and 137 keV.²⁷ In light of the obtained spectrum, this fact suggests that a plasma focus could be investigated as a pulsed hard x-ray source suitable, apart from other applications, for radiotherapy, giving the plasma focus the advantage of emitting higher intensities than radiotherapy tubes, thus allowing for reduced exposure time.

The current research was conducted in a deuterium operated plasma focus, the main reason being the necessity of having a single device capable of being used as a neutron

source as well. Calculations presented in the preceding section show the advantage of using light filling gases to raise V_p and hence to increase the penetration power of the emitted radiation. Nevertheless, the use of other gases or even admixtures, in correspondingly optimized plasma focus devices, allows us to enhance the emission intensity at lower energies, broadening the potentiality these devices exhibit as hard x-ray sources for fast hard x-ray imaging.

ACKNOWLEDGMENTS

This work was supported by PLADEMA-CNEA, IAEA, UBA, and CONICET. Two of the authors (V.R. and L.S.) are also doctoral fellows of CONICET.

- ¹G. Decker and R. Wienecke, *Physica B&C* **82**, 155 (1976).
- ²F. Castillo-Mejia, M. Milanese, R. Moroso, J. Pouzo, and M. Santiago, *IEEE Trans. Plasma Sci.* **29**, 921 (2001).
- ³S. Hussain, R. Ahmad, M. Z. Khan, M. Zakaullah, and A. Waheed, *J. Fusion Energy* **22**, 195 (2003).
- ⁴F. Castillo, J. Herrera, J. Rangel, A. Alfaro, M. Mazza, V. Sakaguchy, G. Espinosa, and J. Golzarri, *Braz. J. Phys.* **32**, 3 (2002).
- ⁵S. Hussain, M. Zakaullah, S. Ali, S. Bhatti, and A. Waheed, *Phys. Lett. A* **319**, 181 (2003).
- ⁶S. Hussain, M. Zakaullah, S. Ali, and A. Waheed, *Plasma Sources Sci. Technol.* **6**, 2296 (2004).
- ⁷S. Hussain, M. Shafiq, R. Ahmad, A. Waheed, and M. Zakaullah, *Plasma Sources Sci. Technol.* **14**, 61 (2005).
- ⁸F. Beg, K. Krushelnick, P. Lichtsteiner, A. Meakins, A. Kennedy, N. Kajumba, G. Burt, and A. Dangor, *Appl. Phys. Lett.* **82**, 4602 (2003).
- ⁹F. Beg, R. Stephens, E. Shipton, D. Haas, G. Andreev, S. Eddinger, and H. Haung, in *6th International Conference on Dense Z-Pinches*, edited by J. Chittenden, AIP Conf. Proc. No. 808 (AIP, New York, 2006), pp. 125–128.
- ¹⁰F. Beg, R. Stephens, H.-W. Xu, D. Haas, S. Eddinger, G. Tynan, E. Shipton, B. DeBono, and K. Wagshal, *Appl. Phys. Lett.* **89**, 101502 (2006).
- ¹¹C. Moreno, A. Clause, J. Martínez, R. Llovera, A. Tartaglione, M. Vénere, R. Barbusza, and M. Del Fresno, in *IX Latin American Workshop on Plasma Physics*, edited by H. Chuaqui and M. Favre, AIP Conf. Proc. No. 563 (AIP, New York, 2001), pp. 300–305.
- ¹²C. Moreno, A. Clause, J. Martínez, R. Llovera, and A. Tartaglione, *Nukleonika* **46**, 33 (2001).
- ¹³V. Raspa, L. Sigaut, R. Llovera, P. Cobelli, P. Knoblauch, R. Vиейtes, A. Clause, and C. Moreno, *Braz. J. Phys.* **34**, 1696 (2004).
- ¹⁴C. Moreno, V. Raspa, L. Sigaut, R. Vиейtes, and A. Clause, *Appl. Phys. Lett.* **89**, 091502 (2006).
- ¹⁵M. Shafiq, S. Hussain, A. Waheed, and M. Zakaullah, *Plasma Sources Sci. Technol.* **12**, 199 (2003).
- ¹⁶H. van Paassen, R. Vandre, and R. White, *Phys. Fluids* **13**, 2606 (1970).
- ¹⁷D. Johnson, *J. Appl. Phys.* **45**, 1147 (1974).
- ¹⁸J. Lee, D. Loebbaka, and C. Roos, *Plasma Phys.* **13**, 347 (1971).
- ¹⁹A. Tartari, A. Da Re, C. Bonifazzi, and M. Marziani, *Nucl. Instrum. Methods Phys. Res. B* **213**, 206 (2004).
- ²⁰F. Castillo, J. Herrera, I. Gamboa, J. Rangel, J. Golzarri, and G. Espinosa, *J. Appl. Phys.* **101**, 013303 (2007).
- ²¹B. Illerhaus, Y. Onel, and J. Goebbels, in *Developments in X-Ray Tomography IV*, edited by U. Bonse, SPIE Proc. No. 5535 (SPIE, Bellingham, WA, 2004), pp. 329–334.
- ²²S. Duclos, *Electrochem. Soc. Interface* **7**, 34 (1998).
- ²³J. Hubbell and S. Seltzer, *X-rays Attenuation Coefficients* (NIST, Washington, DC, 1996), <http://physics.nist.gov/PhysRefData/XrayMassCoef/cover.html>.
- ²⁴CP-G Film datasheet, Agfa-Gevaert N.V., Belgium (2004).
- ²⁵W. H. Press, B. P. Flannery, S. A. Teukolsky, and W. T. Vetterling, *Numerical Recipes in C: The Art of Scientific Computing* (Cambridge University Press, New York, 1988).
- ²⁶S. Lee, in *Small Plasma Physics Experiments II*, Proceedings of the Symposium on Small Scale Laboratory Plasma Experiments, Spring College on Plasma Physics, 1989, edited by S. Lee and P. Sakanaka (World Scientific, Singapore, 1990), pp. 113–169.
- ²⁷F. Verhaegen, A. E. Nahum, S. Van de Putte, and Y. Namito, *Phys. Med. Biol.* **44**, 1767 (1999).